Effects of zero-point phonons and atomic correlations on the electronic properties of crystalline MgO at finite temperatures

2001 J. Phys.: Condens. Matter 13 10873

(http://iopscience.iop.org/0953-8984/13/48/313)

INSTITUTE OF PHYSICS PUBLISHING JOURNAL OF PHYSICS: CONDENSED MATTER

J. Phys.: Condens. Matter **13** (2001) 10873–10887 PII: S0953-8984(01)27644-9

Effects of zero-point phonons and atomic correlations on the electronic properties of crystalline MgO at finite temperatures

Jacob L Gavartin

Department of Physics and Astronomy, University College London, Gower Street, London WC1E 6BT, UK

Received 30 July 2001, in final form 20 September 2001
Published 16 November 2001
Online at stacks.iop.org/JPhysCM/13/10873

Abstract

Utilizing the harmonic approximation, we introduce a simple technique for the generation of ensembles of thermally disordered atomic structures, and calculate for the MgO crystal electron densities of states (DOS) and the on-site potential probability distributions for the ensembles generated within the classical and quasi-classical harmonic approximations, molecular dynamics and uncorrelated Gaussian atomic disorder models. An account of the zero-energy vibrations even at room temperature results in a significant increase in the mean square atomic displacements and, thus, in the probability distributions of the electrostatic potential and ultimately in the extent of the band tails in the electron DOS. We also demonstrate that the correlations in atomic positions affect the electronic structure. We have evaluated directly the on-site potential autocorrelation function (PAF) for all disorder models, as well as the temperature dependence of the PAF. The correlation length, L, is shown to be less than the second nearest neighbour at low temperature and decreasing to below the nearest neighbour distance at $T = 500$ K. The short correlation length obtained in the direct modelling is in agreement with the Urbach–Martienssen rule for the optical absorption edge observed experimentally.

1. Introduction

An atomic disorder in solids profoundly modifies their electronic properties. This effect may become especially important in the electronic and optical properties of crystals with strong electron–lattice interaction. In particular, Citrin and co-authors demonstrated that the electron–phonon coupling leads to a significant broadening of the valence bands of the alkali halide crystals as observed in the x-ray and ultraviolet photoemission spectra [1]. Part of this broadening has been attributed to the local lattice relaxation accompanying the hole localization in the valence band. The temperature-dependent broadening is also shown to

be significant suggesting the importance of the atomic thermal disorder in the electronically ground state. Another phenomenon in the dielectrics linked to the thermal disorder is an exponential temperature dependence of the optical absorption coefficient $\alpha(\hbar\omega)$, known as the Urbach–Martienssen rule [2]:

$$\alpha(\hbar\omega) \sim \exp\{\sigma\beta(\hbar\omega - \hbar\omega_0)\}. \tag{1}$$

Here ω is a circular frequency of the incident light, $\beta = (k_B T)^{-1}$ is the inverse temperature, $\hbar$ and k_B are, respectively, the Planck and the Boltzmann constants, and ω_0 and σ are the fitting parameters, which themselves may depend on temperature. Extensive theoretical studies of the microscopic origin of the Urbach–Martienssen rule gave rise to a qualitative picture which can be summarized as follows [3]. A disorder in the positions of atomic nuclei causes the fluctuations in the electron potential Δv, which in turn result in the appearance of tails at the band edges of the electronic density of states (DOS), often referred to as Lifshitz or band tails [4]. A decay of these tails into the band gap region is predominantly exponential with the exponent being proportional to the variance σ^2 of the potential probability distribution $g(v)$ [5], Electron states in Lifshitz tails are characterized by the progressively increasing degree of localization as the eigenvalues extend into the band gap. It has been suggested that the contribution of the states in the Lifshitz tails to the optical absorption is responsible for the exponential behaviour of the absorption coefficient $\alpha(\hbar\omega)$. Sa'Yakanit *et al* [6] argued that the exponential shape of the band tails alone is sufficient for the description of the exponential behaviour of $\alpha(\hbar\omega)$. However, Dow and Redfield [7] and also Toyozawa and Sumi [8] pointed out that both the convolution of the occupied and empty bands and the optical transition probabilities may play a crucial role in certain systems. In particular, Sumi and Toyozawa [8] studied the excitonic effect on the optical absorption coefficient in narrow-band crystals.

An appearance of the band tails can be qualitatively explained using a model tight-binding Hamiltonian with diagonal Gaussian disorder [9]. In this approach the perturbation potential V of the perfect crystal Hamiltonian, H_0, introduces a zero-mean Gaussian disorder in the on-site matrix elements. However, the usefulness of the model Hamiltonian approach is limited when the *quantitative* characterization of disorder in specific systems is required.

First, approximations must be made about the shape of the probability distribution, $g(v)$, of the potential felt by the electrons and about the variation of this distribution with temperature. The important prediction of all mean field linear theories is that the potential probability distribution is Gaussian [10]. Although this is found to be the case in a number of dielectric systems [11–13], the validity of the linear approximation to different types and levels of disorder ought to be verified for specific systems [14].

In the case of thermal disorder, a ground state electronic structure can be considered as adiabatically following the atomic trajectories. Hence, the probability distribution for the potential is uniquely characterized by the distributions in atomic displacements. With regard to the modelling of specific systems, two issues are of interest. First, as evidenced by the x-ray, ultraviolet and optical spectroscopy experiments [15], band tails in polar dielectrics persist even at very low temperatures. Therefore, it has been argued that low temperature band tails may originate from extrinsic (impurities and self-defects) rather than from intrinsic thermal disorder [16]. At the same time it is recognized [7] that the amplitudes of the potential fluctuations in pure polar dielectrics will depend on the optical phonon population, which at sufficiently low temperatures obeys quantum rather than classical statistics. In crystals with high Debye temperature, the zero-point phonons may significantly contribute to the atomic mean square displacements [17] (MSD), thus affecting the potential fluctuations and

the electronic band tails even near absolute zero temperatures. We note, in passing, that the vast majority of the dynamic simulations consider atomic motion classically (even though the forces upon atoms may be considered quantum mechanically as, for example, in the Born–Oppenheimer or Car–Parrinello *ab initio* molecular dynamics). We shall demonstrate that atomic disorder due to zero-point phonons in crystalline MgO results in the appearance of observable band tails, and the effect of quantum statistics for the phonons is still strong at room temperature.

The second related issue concerns the fact that the electrostatic potential fluctuations on the spatially separated lattice sites correlate. This effect is neglected in the diagonal disorder models. It is known, however, that the correlations between the potential fluctuations on distant atoms have a significant effect on the electronic structure. Halperin and Lax [18] first pointed out that the shape of the electronic DOS, $\rho(E)$, deep in the band tail region is coupled exponentially to the disorder correlation length, L:

$$\ln \rho(E) \propto E^{n(L)}$$

where in three-dimensional systems n varies between $1/2$ and 2 as L changes from 0 (white noise limit) to ∞ (translational order). They also demonstrated that n is bound within the above limits in the systems with electronically screened Coulomb interaction. An exact account of the potential correlations on the Lifshitz tails has been obtained for the so-called correlated Gaussian random potential [19], where various monotonic isotropic decay forms for the potential autocorrelation function (PAF) $B(r) = \langle v(0)v(r)\rangle_0$ were considered. These calculations revealed that for the Urbach rule to hold, the disorder correlation length must be sufficiently short, i.e. not exceeding one lattice constant. To the best of our knowledge, no direct evaluations have been made of thermal disorder correlation length in crystalline polar systems and its influence on the band structure. Towards this goal Koslowski first calculated the band tails in molten salts [11] within the topological and Madelung potential disorder. He concluded that the topological disorder mainly shifts the bands, while, together with the potential disorder, it results in the appearance of the band tails. However, the question of the potential fluctuation correlation length has not been discussed.

In this paper we present the first attempt to calculate the potential autocorrelation function directly for a thermally disordered crystalline dielectric. We consider crystalline MgO as a case study and calculate the electron DOS, Madelung potential probability distributions and potential autocorrelation functions for statistical ensembles of atomic configurations generated within different models of thermal disorder. Magnesium oxide is a wide-gap dielectric with a rock salt structure. It is characterized by a high Debye temperature [20] ($\theta_D = 941$ K) and retains its harmonic properties to relatively high temperatures [21].

First, we consider an ensemble of instantaneous atomic configurations generated within classical molecular dynamics (MD) simulations. In order to account for the effects of zero-point phonon disorder, we generate the ensemble of configurations within a quasi-classical harmonic approximation (QHA). To verify the applicability of the harmonic approximation we consider an ensemble generated within the classical harmonic approximation (CHA) and compare its atomic and electronic properties with those of the ensemble generated by the classical MD. And finally, to discuss the effects of the atomic correlations, we generate the ensemble of atomic configurations within the uncorrelated Gaussian atomic disorder model (UGAD).

We then calculate the electronic structure of the ensembles thus generated, and proceed with the evaluation of the probability densities of the on-site electrostatic potential and the potential autocorrelation functions $B(r)$ in the above models.

2. Calculation procedure

2.1. Shell model Hamiltonian

We utilize the Born–Oppenheimer approximation, that is, for each instantaneous atomic configuration considered, we calculate its electronic ground state ignoring the kinetic energies of the atomic nuclei.

To study the effect of thermal disorder, first the ensembles of the atomic configurations must be generated so that their electronic properties can be calculated and statistically averaged.

To generate the disordered atomic configurations we employ the shell model interatomic potentials developed by Stoneham and Sangster [23] and utilized in the general utility lattice program (GULP) code [24] for the lattice dynamics and MD simulations. In this model the ions interact electrostatically and elastically via the pairwise central potentials of the Buckingham form. The ionic charges are taken to be $\pm 2e$ for the Mg and O ions and cations are considered unpolarizable. The parameters for the short-range interaction were fitted to reproduce the experimental lattice geometry and the dielectric and elastic constants. This set of potentials has been extensively tested for the MD modelling by Fincham and co-authors [21] and was found to predict fairly well the phonon dispersion, the dielectric and elastic constants at ambient pressures and temperatures, as well as the volume thermal expansion and compressibility of crystalline MgO in a wide interval of temperature and pressure.

2.2. Models for thermal disorder

In all our calculations we consider a cubic supercell of 512 atoms ($4 \times 4 \times 4$ extension of the crystalline unit cell of eight ions) subject to periodic boundary conditions.

First we consider the ensemble of atomic configurations generated by the classical MD. We undertake a microcanonical MD (constant number of particles, volume and the total energy (NVE)) at temperatures of 100, 300 and 500 K. Shells on the oxygen atoms are treated adiabatically, i.e. at each MD time step they are relaxed to their equilibrium positions. In all calculations, the time step has been chosen as 0.5 fs, which assured no drift in the total energy of the system within the time range of up to 20 ps.

The zero-phonon effects in atomic disorder can be introduced within the harmonic approximation, according to which a displacement operator of the individual atom i from the lth unit cell in the Cartesian direction α from its perfect lattice position $\boldsymbol{R}(li)$ is expressed in terms of the displacement operators of the crystal normal modes, $\hat{A}(\boldsymbol{q}j)$,

$$\hat{u}_{i\alpha}(l) = \sum_{\boldsymbol{q}j} \left(\frac{\hbar}{2M_i \mathcal{N} \omega(\boldsymbol{q}j)} \right)^{1/2} e(i\alpha \mid \boldsymbol{q}j) \exp\{i\boldsymbol{q}\boldsymbol{R}(li)\} \hat{A}(\boldsymbol{q}j) \tag{2}$$

where $\mathcal{N}$ is the number of unit cells, M_i the mass of the atom i, $\omega(\boldsymbol{q}j)$ the harmonic frequency of the phonon specified by the wave vector $\boldsymbol{q}$ and the branch number j, and $e(i\alpha \mid \boldsymbol{q}j)$ is the $i\alpha$ component of the corresponding eigenvector.

In what follows, we consider a supercell assumed to be large enough to contain all the physically important phonons. Then, the expression for atomic diplacement (2) reduces to the central supercell only, that is, to the conditions $\boldsymbol{q} = 0, l = 0, \mathcal{N} = 1$,

$$\hat{u}_{i\alpha} = \sum_{j} \left(\frac{\hbar}{2M_i \omega_j} \right)^{1/2} e(i\alpha \mid j) \hat{A}_j \tag{3}$$

where the subscript j now numerates all the Γ-point phonons within the supercell. Using the orthonormality conditions for the eigenvectors $e(i\alpha \mid j)$ the expression for the atomic mean square displacement is obtained

$$\left\langle u_{i\alpha}^2 \right\rangle = \frac{\hbar}{2M_i} \sum_j e^2(k\alpha \mid j) \frac{\left\langle A_j^2 \right\rangle}{\omega_j} \tag{4}$$

where angular brackets indicate the quantum mechanical average.

In order to generate atomic displacements $u_{i\alpha}$, we first make the quasi-classical approximation; that is, we replace the operators in equation (3) by their expectation values. Next, we assume that the system of interest is at thermodynamic equilibrium at temperature T, and consider statistical distributions of the individual phonon coordinates A_j. In the QHA approximation the coordinate probability distribution $P(A_j)$ is given in terms of the eigenfunctions $\Psi_{nj}(A)$ of the corresponding harmonic oscillator

$$P_Q(A_j) = \frac{1}{Z_j} \sum_{n=0}^{\infty} \mathrm{e}^{-\beta\hbar\omega_j(n+\frac{1}{2})} |\Psi_n(A_j)|^2 \tag{5}$$

where the subscript Q refers to the quantum statistics case; Z_j is the partition function for the ensemble of harmonic oscillators with frequency ω_j at temperature T:

$$Z_j = \mathrm{Tr}\left[\mathrm{e}^{-\beta\hbar\omega_j(n+\frac{1}{2})}\right]. \tag{6}$$

The summation in the equation (5) can be carried out analytically using the explicit form for the eigenfunctions $\Psi_n(A_j)$ and the generating function method for the Hermite polynomials [22]. The result is

$$P_Q(A_j) = \frac{1}{\sqrt{2\pi}\sigma_Q} \exp\left(-\frac{A_j^2}{2\sigma_Q^2}\right) \tag{7}$$

with

$$\sigma_Q^2 = \frac{\hbar}{2\omega_j} \coth\frac{\beta\hbar\omega_j}{2}. \tag{8}$$

Therefore, the coordinate probability distribution for the phonon j is Gaussian with the variance given by equation (8). Recalling that the mean square displacement of the phonon coordinate $\left\langle A_j^2 \right\rangle$ is proportional to the mean phonon population $\bar{n}_j$, which at thermal equilibrium obeys the Bose–Einstein statistics, one can verify that

$$\sigma_Q^2 = \frac{\hbar}{2\omega_j} \left\langle A_j^2 \right\rangle. \tag{9}$$

Similarly, assuming *classical statistics* for phonons, one can show that in the harmonic approximation the probability distribution for the phonon coordinate is also Gaussian (equation (7)) but with the classical variance σ_C^2:

$$\sigma_C^2 = \left(\beta\omega_j^2\right)^{-1}. \tag{10}$$

Equations (7)–(10) are the quantitative manifestations of Bloch's second theorem [25] stating that the coordinate distribution of an ensemble of harmonic oscillators (classical or quantum) is Gaussian. The variance σ_Q^2 reduces to σ_C^2 in the limit of high temperature or low frequency ($\beta\hbar\omega_j \ll 1$).

Taking into account the above considerations, we adopt the following procedure for the generation of atomic disorder in a harmonic system:

1. Given the system's shell model Hamiltonian, solve the lattice dynamic problem (subject to the periodic boundary conditions), that is, calculate the eigenvectors $e(j \mid k\alpha)$ and frequencies ω_j. This step is undertaken using the GULP code [24].
2. For each phonon j generate a random phonon coordinate A_j from the Gaussian distribution with a zero mean and variance σ^2 defined by equations (8) or (10) for the quantum or classical approximations, respectively.
3. Given the coordinates of all the phonons A_j, calculate the Cartesian displacements $u_{k\alpha}$ for each atom k according to equation (3).

The classical harmonic approximation can be critically tested by comparison of the atomic MSDs calculated using equation (4) with the values obtained by a direct MD simulation.

The outlined method allows generation of quantum or classical ensembles of atomic configurations by utilizing the system's detailed dynamic information (including interatomic correlations).

It is instructive to ask to what extent the electronic structure is sensitive to the correlations in atomic positions. On this account we examine an ensemble of atomic configurations generated in the assumption of *uncorrelated Gaussian atomic disorder*. It can be demonstrated [17] that the probability density for the atomic displacement of the individual atoms is Gaussian:

$$P(u) = \frac{1}{\sqrt{2\pi \left\langle u_j^2 \right\rangle}} \exp\left(-\frac{u^2}{2\left\langle u_j^2 \right\rangle} \right) \tag{11}$$

where $\langle u_j^2 \rangle$ is the MSD of the atomic species j. Provided that each atom is considered as an independent oscillator (as in the Einstein solid), individual atomic displacements can be drawn independently from a Gaussian distribution (11) with the MSDs, $\langle u_j^2 \rangle$, calculated within QHA, CHA or MD simulations. Note that although the correlations in the atomic positions are neglected in the UGAD model, some correlations between the fluctuations of the electrostatic potential on remote lattice sites are still present due to the self-consistent character of the electronic structure calculations.

2.3. Electronic structure calculations

To calculate the electronic structure of the ensembles of atomic configurations thus generated, we use a supercell approach and the semi-empirical LCAO Hartree–Fock method at the level of intermediate neglect of differential overlap (INDO), implemented in the SYM–SYM package [26]. INDO parameters were fitted to represent the geometry of the MgO molecules, the lattice constant, the valence band and the energy gap widths of the perfect MgO crystal [27]. In the LCAO approach the eigenfunctions $\psi_\varepsilon(\boldsymbol{r})$ are expressed as a linear combination of atomic orbitals (AO): (we consider the valence s-orbitals on magnesium ions and s- and p-valence orbitals on oxygen ions)

$$\psi_\varepsilon(\boldsymbol{r}) = \sum_{i\alpha} c_{i\alpha}(\varepsilon)\phi_\alpha(\boldsymbol{r}) \tag{12}$$

where i enumerates the atoms and α specifies the atomic orbital, $c_{i\alpha}(\varepsilon)$ are the ortho-normal components of the eigenvector belonging to the eigenvalue ε. Eigenvectors, $c_{i\alpha}(\varepsilon)$, and eigenvalues, ε, are obtained from the self-consistent solution of the Hartree–Fock equation. An electron DOS is then constructed by Gaussian broadening of the one-electron spectra ($\sigma =$ 0.1 eV).

Besides the one-electron eigenstates $\psi_\varepsilon(\boldsymbol{r})$, we also calculate effective ionic charges $\{q_i\}$ (using the modified Löwdin population analysis [28]) and on-site electrostatic potentials $\{v_i\}$ resulting from the charge distributions. These data are used to generate the probability distributions of the electrostatic potential, $g_s(v)$,

$$g_s(v) = \left\langle \delta\left(\sum_{j(\neq i)} \frac{q_j}{|\boldsymbol{r}_i - \boldsymbol{r}_j|} - v \right) \right\rangle_{i\in s} \tag{13}$$

where $\delta(x - x_0)$ is a Dirac δ-function, q_j and $\boldsymbol{r}_j$ denote the charge and the position vector of an ion j, respectively, and j runs over all the ions in the system except ion i, s denotes the sublattice (s = Mg or O), and the angular brackets indicate the ensemble average over the atomic sites belonging to the sublattice s. Note that due to the self-consistent character of the solution, ionic charges q_j fluctuate together with the on-site Madelung potential. Thus a disorder in atomic positions causes fluctuations of both the electrostatic potential and effective ionic charges [14].

Given the on-site electrostatic potentials $\{v_i\}$ on the ions located at points $\boldsymbol{r}_i$, we introduce the spherically averaged on-site potential autocorrelation function,

$$B(r_z) = \langle v(0)v(r)\rangle_0 - \langle v^2\rangle = \frac{1}{\langle v^2\rangle} \sum_{ij} \Delta v(\boldsymbol{r}_i)\Delta v(\boldsymbol{r}_j)\theta(r_{ii'} - r_{1z})\theta(r_{2z} - r_{ii'}) \tag{14}$$

where r_z indicates the radius of the coordination sphere z, around which the function is evaluated, $\Delta v(\boldsymbol{r}_i) = \sum_{k(\neq i)} \frac{q_k}{|\boldsymbol{r}_i - \boldsymbol{r}_k|} - \langle v\rangle$ is a fluctuation (deviation from the sublattice average) of the electrostatic potential on the atomic core with a position vector $\boldsymbol{r}_i$. Index i runs over all the lattice sites, and the product of the Heaviside step functions $\theta(x - r_{1z})\theta(r_{2z} - x)$ ensures that for a chosen lattice site i, the averaging is taken over the spherical shells containing all the atoms from a given coordination sphere, z (e.g. for the first coordination sphere, we choose $r_{11} = a_0/2$ and $r_{21} = a_0(1 + \sqrt{2})/2$, where a_0 is the nearest Mg–O distance in the perfect lattice, etc). Note that the mean values of the on-site potentials on the cation and anion sublattices are equal in absolute value, although their variances may differ [14]. Therefore, we define $\langle v^2\rangle$ in equation (14) as an average variance for the anion and cation sublattices.

3. Results

3.1. Atomic mean square displacements

The atomic MSDs calculated according to equation (4) for the CHA and QHA models are shown in figure 1 as a function of temperature. The MSDs predicted by the classical MD simulations at $T = 100$, 300 and 500 K are also shown. We note that in the QHA and CHA models, atomic MSDs are calculated in the approximation of the temperature-independent frequency spectrum. Thus, an effect of thermal lattice expansion on atomic MSDs is neglected. For the sake of comparison all the MD calculations are also made at the same constant volume. The following main features result from these calculations:

1. Atomic mean square displacements are different for different sublattices, with the lighter oxygen atoms having larger MSD.
2. The MSD obtained from the MD and those from the CHA are very similar. This justifies the applicability of the harmonic approximation in the temperature range studied.
3. Accounting for zero-point phonons in the QHA model results in a significant increase of atomic MSDs with respect to those predicted by classical approximation. The MSDs

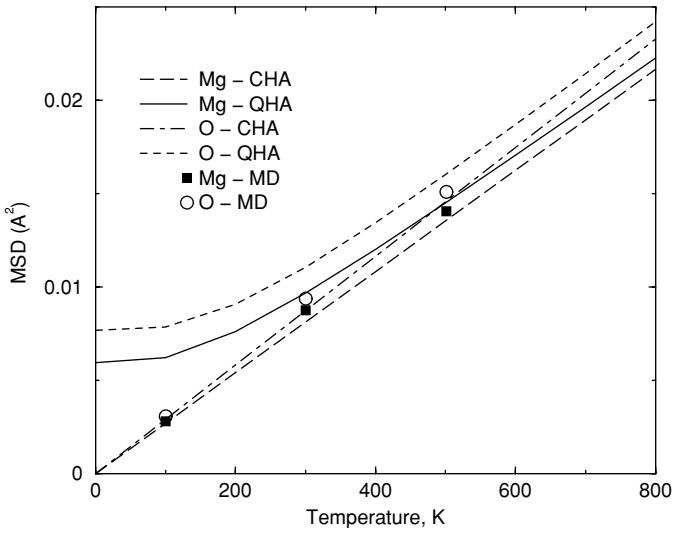

Figure 1. Temperature dependence of mean square ionic displacements calculated for magnesium and oxygen ions within the classical and quantum harmonic approximations, and directly from MD.

calculated with the QHA model are approximately twice the classical values at 100 K and a difference is still noticeable at $T = 500$ K.

3.2. Probability distributions for the on-site potential and electron DOS

The larger atomic MSDs affect the probability distributions of the on-site electrostatic potential for the magnesium and oxygen sublattices. The probability distributions (13) averaged over the sets of 6 to 16 atomic configurations generated within the MD, QHA and UGAD models at $T = 300$ K are shown in figure 2. In the UGAD approach (equation (11)) the atomic MSDs obtained within the classical MD simulations at this temperature are used.

All the models predict the on-site potential probability distribution to be Gaussian with the mean value close to that of the on-site electrostatic potential in the perfect lattice. However, the distribution variances $\langle v^2 \rangle$ differ significantly. As expected (from larger atomic MSDs) the distribution predicted by the QHA is wider than that obtained with the classically generated configurations. Furthermore, the variance of the potential probability distribution resulting from the UGAD model is a factor of 1.7 larger than that predicted by classical MD, albeit the same mean square atomic displacements are used in both models. Evidently, an overestimation of the fluctuations of the on-site electrostatic potential in the UGAD model results from the neglect of the correlations in the atomic positions. This strong effect can be understood by considering the atomic structures statistically. The different atomic configurations contribute to ensemble averaging with the Boltzmann factor reflecting the probability of their realization at a given temperature. When the probability factor is neglected (as in the case of the UGAD model), the highly improbable vibrational excitations become dominant in the ensemble averages. We find that the average energy per MgO molecule in the UGAD ensemble is 0.03 eV higher than in the ensemble generated by the MD simulations. An evidently strong correlation effect in MgO is related to the long phonon life times in this material even at relatively high temperatures.

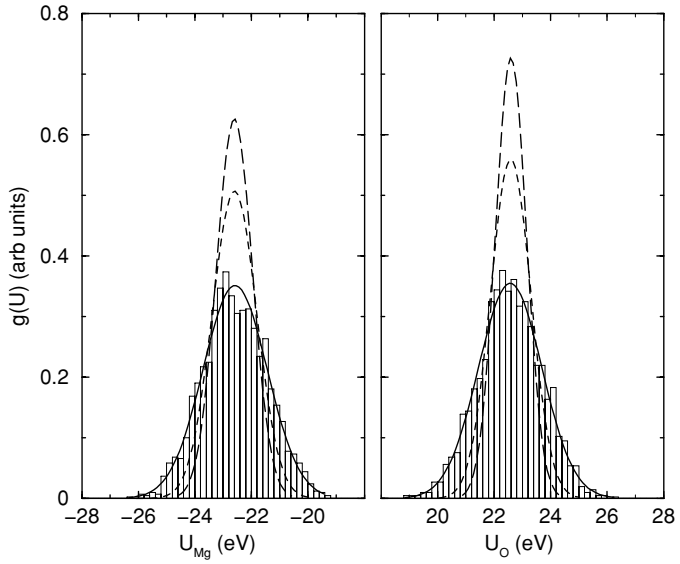

Figure 2. On-site electrostatic potential distributions for the magnesium (left) and oxygen (right) sublattices derived for three models at 300 K: UGAD (solid curves) with the atomic MSD equal to that in classical MD; QHA (dashed curves); classical MD (long-dashed curves). The curves are the Gaussian approximations to the distributions, the actual histograms of the raw data for the UGAD model are also shown for comparison.

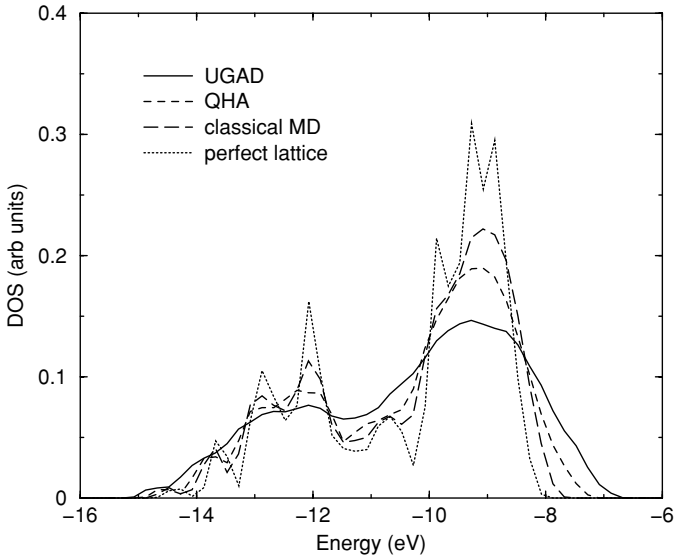

Figure 3. The valence band densities of states, calculated for the representative atomic structures corresponding to the UGAD, QHA and classical MD models at 300 K. The DOS of the perfect MgO lattice is also shown for comparison. The broadening parameter is 0.1 eV in all calculations.

As discussed in section 1, a finite width of the distribution of electrostatic potential affects the electronic structure. The valence band electronic DOS calculated for the representative atomic configurations generated by different models at $T = 300$ K are shown in figure 3. It

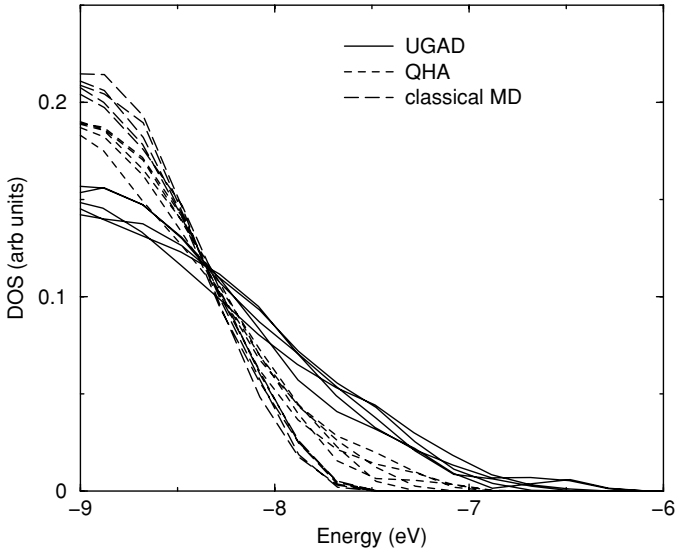

Figure 4. A blow-up of figure 3 showing the valence band tail area of the DOS for five representative configurations in each model.

is seen that the tail in the DOS predicted by the QHA is more than 0.5 eV longer than that of the classically disordered system. The tail in the DOS of the uncorrelated system is even longer. To demonstrate a degree of statistical scatter in electronic DOS, we depict in figure 4 the tails of the valence band DOS calculated for five different atomic configurations within each model. Clearly, the variations in DOS calculated for atomic configurations generated by the same model are smaller than the DOS variations between the different models.

3.3. Potential autocorrelation function

The potential autocorrelation function (14) for up to the sixth coordination shell has been evaluated for the classical MD, QHA and UGAD ensembles, and the results for $T = 300$ K are depicted in figure 5. It is evident that different models predict different decays for the PAF. In order to quantify these differences we have modelled our numerical data by two analytical forms for PAF used in the literature: (i) the exponential decay model

$$B_1(r) = \langle v^2 \rangle \exp\left\{ -\left(\frac{r}{R_1} \right)^{m_1} \right\} \tag{15}$$

and (ii) the power decay model

$$B_2(r) = \langle v^2 \rangle \left[1 + \left(\frac{r}{R_2} \right)^2 \right]^{-m_2} . \tag{16}$$

The exponential model is a generalization relevant for those disordered systems where the fluctuations of the potential are stipulated by the *randomly* distributed charged impurities interacting via potentials of different range (e.g. $m = 1$ corresponds to the Coulomb-screened potential model [18], $m = 2$ represents the Gaussian model [19], etc). The power decay model, $B_2(r)$, originates from the models for topological and thermal disorder in polar dielectrics [19].

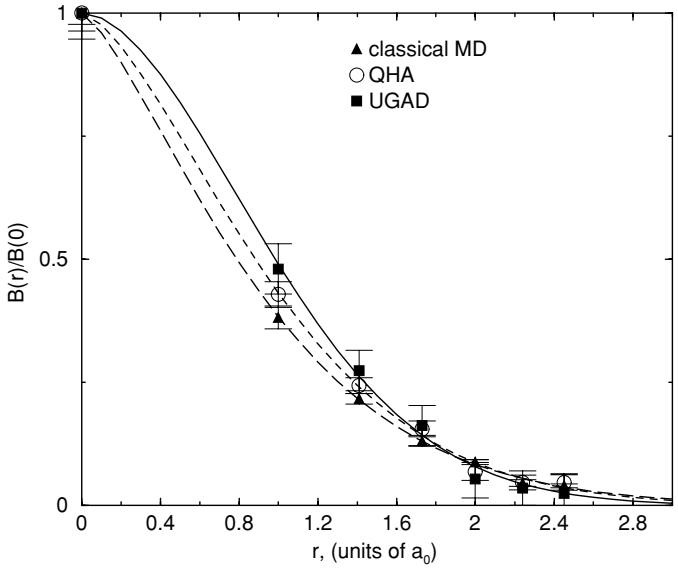

Figure 5. The autocorrelation function for the on-site electrostatic potential (14) calculated for the UGAD, QHA and classical MD models at 300 K. The curves (respectively solid, dashed and long-dashed) represent the best fits by the exponential decay function (15) with the parameters listed in table 1.

Table 1. Fitted parameters for the potential autocorrelation function in the forms $B_1(r) = \langle v_0^2 \rangle \exp\{-(\frac{|r|}{R_1})^{m_1}\}$ and $B_2(r) = \langle v_0^2 \rangle [1 + (\frac{r}{R_2})^2]^{-m_2}$ for the UGAD model (300 K), QHA (300 K), and classical MD (100, 300 and 500 K). The statistical uncertainty for $\langle v_0^2 \rangle$ is shown in brackets. Parameters R_i and the correlation length L_i are in units of the MgO lattice constant a_0.

Model	$\langle v_0^2 \rangle$ (eV^2)	R_1 (a_0)	m_1	L_1 (a_0)	R_2 (a_0)	m_2	L_2 (a_0)
UGAD 300 K	1.22 (0.05)	1.202	1.833	0.89	3.85	10.714	0.90
QHA 300 K	0.58 (0.04)	1.120	1.539	0.94	1.75	2.915	1.03
MD 100 K	0.12 (0.01)	1.060	1.335	1.02	1.25	1.842	1.28
MD 300 K	0.35 (0.02)	1.030	1.372	0.96	1.32	2.072	1.15
MD 500 K	0.61 (0.05)	1.022	1.651	0.81	2.15	4.862	0.83

The best-fit parameters R and m for the models (15) and (16) are listed in table 1 together with the calculated variances $\langle v^2 \rangle$. We observe that both functional forms fit the calculated data with almost the same accuracy (the exponential form on average performs marginally better). As seen in figure 6, the exponential model (15) and the power model (16) decay almost identically in the region between one and three lattice constants. At the same time, the values of the decay parameters R in the two models are very different. We note that, in general, the parameter R alone does not reflect the characteristic correlation length for the fluctuations of the potential. For example, one can show that in the screened Coulomb potential model ($m = 1$ in equation (15)), the parameter R is equal to the screening length, thus characterizing the properties of the medium rather than the correlation length (the screened Coulomb model assumes *no correlations* between the fluctuations of the potential). In the search for a universal fluctuation length parameter (which will generally depend on both R

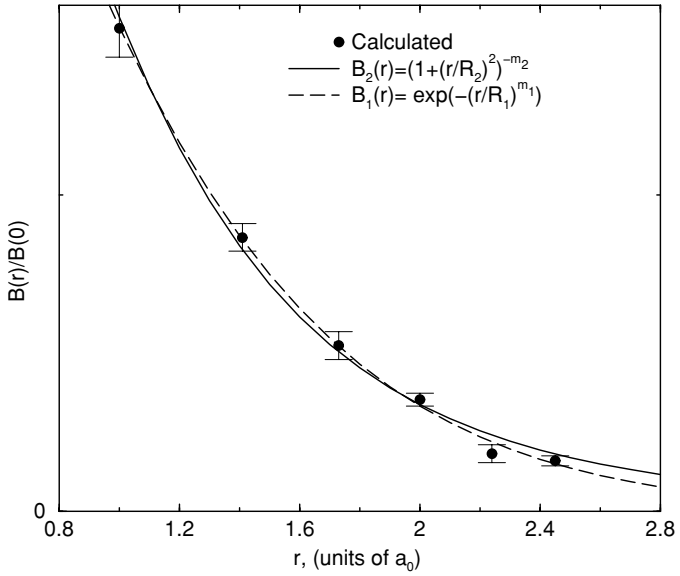

Figure 6. The potential autocorrelation function as calculated with the MD model at $T = 300$ K (circles). The lines represent the best fits to the PAF models given by equations (15) and (16) with the parameters listed in table 1.

and m), we follow the work of John and co-authors [19] and introduce a *natural correlation length*, L, of the PAF:

$$L^2 = \frac{\int_0^\infty r^2 B(r)\,\mathrm{d}r}{\int_0^\infty B(r)\,\mathrm{d}r}. \tag{17}$$

Straightforward integration for the power exponential model (15) gives the following relation between L and parameters R_1 and m_1:

$$L_1 = R_1 \sqrt{\frac{\Gamma\left(3m_1^{-1}\right)}{\Gamma\left(m_1^{-1}\right)}} \tag{18}$$

where $\Gamma(x)$ is a gamma function. The values of the correlation length, L, calculated for the exponential (15) and power decay (16) models, are summarized in table 1.

We have also studied the temperature dependence of PAF calculated in the classical MD model within the temperature range 100–500 K (table 1). We find the potential variance $\langle v^2 \rangle$ to be proportional to temperature as expected in the classical harmonic approximation. At the same time both models for PAF predict a decrease of L with temperature. Also the values of L predicted by the two models are similar. We note in passing that the R parameter slightly decreases with temperature for a power exponential model and increases for the power decay model (table 1), confirming that this parameter alone does not characterize the decay behaviour of the autocorrelation function.

4. Discussion

We have examined the electronic properties of different models of thermal disorder in an otherwise perfect MgO crystal. First we observe that all the methods predict the on-site

electrostatic potential distribution to be of Gaussian shape. The assumption of Gaussian form for the potential probability distributions is at the heart of most tractable models of disorder, including those for heavily doped semiconductors [29], Coulomb liquids [10, 11], and statically and dynamically disordered dielectrics [3, 18, 19]. It has been demonstrated [10] that the Gaussian approximation for the probability distribution follows from the linear approximation in mean field theories [10], which is apparently well-obeyed in MgO as suggested by our calculations. Interestingly, a Gaussian distribution is predicted even within the UGAD approximation, implying that the atomic correlations do not affect the general shape of the potential distribution. We have argued elsewhere [14] that this is a consequence of the flatness of the on-site electrostatic potential near the perfect crystal sites of cubic binary dielectrics.

At the same time, the variance of the potential distribution, predicted by different models, varies significantly, in that the classical model significantly underestimates, while the UGAD approximation overestimates the distribution width $\langle v^2 \rangle$. We have also verified that the variance of the distribution increases linearly with temperature [14]. At $T = 300$ K the QHA model predicts the standard deviation of 0.76 eV (table 1). This is significantly larger than the value of 0.13 eV estimated by Dow and Redfield [7] in the assumption that only the Γ-point LO phonon contributes to the $\langle v^2 \rangle$. This large discrepancy suggests that the contribution from other phonons is important.

The question, what phonons couple most to the electrons, has been widely discussed in the literature and remains largely open. Long- and short-wave optical phonons have been suggested for polar crystals (see the paper by Dow and Redfield for a detailed discussion [7]). Also, the possible role of acoustic phonons in polaron formation has been discussed by Toyozawa [30]. We note that the problem of selectivity of phonons in electron–phonon coupling can be addressed systematically within the QHA approach, presented in this paper, by generating ensembles of configurations with only selected phonons being populated. The work in this direction is currently under way.

Although the electron DOSs calculated in this study are not sufficiently accurate to investigate directly the asymptotic behaviour of the band tails, $\rho(E)$, we have demonstrated that the shape of the band tails is quite sensitive to the details of the phonon structure (fluctuation correlations) and the phonon statistics (fluctuation amplitudes) incorporated in a particular model of disorder. We have not been able to discriminate between the exponential and power decay models for the PAF in MgO crystal. Despite possibly different underlying physics behind these models, we suggest that the recovery of the exact form of PAF from the shape of the band tails is beyond the reach of any conceivable experiment. However, we identified and directly estimated for MgO the two main parameters of the PAF, namely the variance of the probability distribution $\langle v^2 \rangle$ and the disorder correlation length, L. As seen in table 1, the exponential and the power decay models predict very similar correlation length, which does not exceed the second neighbour distance at low temperatures and decreases to below the nearest neighbour distance at room temperature.

Our study suggests that zero-point phonons significantly affect atomic disorder. Therefore, intrinsic thermal disorder in polar dielectrics may result in the appearance of the observable band tails at low temperature. It is interesting to note that, since the potential variance $\langle v^2 \rangle$ is known to increase linearly with temperature, a temperature dependence of the correlation length, L, can, in principle, be experimentally probed by recovering the parameters for PAF, e.g. from the temperature dependence of the valence band tail as observed in the x-ray or UV spectroscopy. Also, an analytical model for PAF in polar dielectrics can be derived in the harmonic limit and compared with the experiment.

Finally, in this paper we discussed only the influence of thermal disorder on the shape of band tails. However, it is well established that the optical properties of the polar dielectrics

are not described by the ground state DOS alone. The convolution effects (the joint density of states) of the initial and final states as well as the optical transition matrix elements have been suggested as important [7]. The latter may be especially significant recalling that the single particle states in the band tails are progressively more localized and the overlap between the states in the tail of the valence and conduction bands may become small. Also, the excitonic effects may influence the behaviour of the optical absorption edge of narrow band materials [8]. To account for these effects, methods must be employed which can reliably reproduce the self-trapping process. In this respect, some of the problems with the existing electronic structure methods have been highlighted elsewhere [14, 31].

In summary, we have considered the effect of zero-point phonons and atomic correlations on the electronic structure of thermally disordered MgO. We conclude that both effects are substantial even at room temperature.

Acknowledgments

The funding by the Leverhulme Trust is gratefully acknowledged. Calculations have been performed on the National CRAY T3E supercomputer facility provided by the Materials Chemistry Consortium, UK and on the Bentham computer at the HiPerSPACE Centre at the University College London. I am grateful to A L Shluger, A M Stoneham, A A Sokol, L N Kantorovich and M Gillan for stimulating discussions.

References

[1] Wertheim G K, Rowe J E, Buchanan D N E and Citrin P H 1995 *Phys. Rev.* **51** 13 675
[2] Urbach F 1953 *Phys. Rev.* **92** 1234
Martienssen W 1957 *J. Phys. Chem. Solids* **2** 257
[3] Soukoulis C M and Economou E N 1999 *Waves Random Media* **9** 255
[4] Lifshitz I M 1964 *Adv. Phys.* **13** 483
[5] Economou E N, Soukoulis C M, Cohen M H and Zdetsis A D 1985 *Phys. Rev.* B **31** 6172
[6] Sa-Yakanit V and Glyde H R 1987 *Comment. Condens. Matter Phys.* **13** 35
[7] Dow J D and Redfield D 1972 *Phys. Rev.* B **5** 594
[8] Sumi H and Toyozawa Y 1971 *J. Phys. Soc. Japan* **31** 342
Toyozawa Y 1971 *J. Phys. Soc. Japan* **30** 1555
Sumi H and Sumi A 1987 *J. Phys. Soc. Japan* **56** 2211
[9] Ziman J 1971 *Models of Disorder: The Theoretical Physics of Homogeneously Disordered Systems* (Cambridge: Cambridge University Press)
[10] Logan D E and Siringo F 1992 *J. Phys.: Condens. Matter* **4** 3695
[11] Koslowski T 1996 *Ber. Bunsenges. Phys. Chem.* **100** 95
[12] Koslowski T 2000 *J. Chem. Phys.* **113** 10 703
[13] Koslowski T and Logan D E 1994 *J. Phys. Chem.* **98** 9146
[14] Gavartin J L and Shluger A L 2001 *Phys. Rev.* B at press
[15] Tomiki T, Miyata T and Tsukamoto H 1973 *Z. Naturf.* a **29** 145
[16] Luschik A 2000 Private communication
[17] Kosevich A M 1999 *The Crystal Lattice: Phonons, Solitons, Dislocations* (New York: Wiley)
[18] Halperin B I and Lax M 1966 *Phys. Rev.* **148** 722
[19] John S S, Soukoulis C M, Cohen M H and Economou E 1986 *Phys. Rev. Lett.* **57** 1777
John S, Chou M Y, Cohen M H and Soukoulis C M 1988 *Phys. Rev.* B **37** 6963
[20] Barron T H K, Berg W T and Morrison J A 1959 *P. Roy. Soc. Lond. A Mat., V.* **250** 70
[21] Fincham D, Mackrodt W C and Mitchell P J 1994 *J. Phys.: Condens. Matter* **6** 393
[22] Kubo R and Toyozawa Y 1955 *Prog. Theor. Phys.* **13** 160
[23] Stoneham A M and Sangster M J L 1985 *Phil. Mag.* B **52** 717
[24] Gale J D 1997 *J. Chem. Soc. Faraday Trans.* **93** 69
[25] Bloch F 1932 *Z. Phys.* **74** 265

[26] Kantorovich L N, Stashans A, Kotomin E A and Jacobs P W M 1994 *Int. J. Quantum Chem.* **52** 1177
[27] Stefanovich E V, Shidlovskaya E K, Shluger A L and Zakharov M A 1990 *Phys. Status Solidi* b **160** 529
[28] Pople J and Beveridge D 1970 *Approximate Molecular Orbital Theories* (New York: McGrow-Hill)
[29] Bonch-Bruevich V L and Mironov A G 1962 *Sov. Phys.–Solid State* **3** 1219
[30] Toyozawa Y 1961 *Prog. Theor. Phys.* **26** 29
[31] Gavartin J L and Shluger A L 2001 *Radiation Effects and Defects in Solids* at press